Benha Journal of Applied Sciences (BJAS) **print: ISSN 2356–9751**
Vol. (9) Issue (3) (2024), (197-206) **online: ISSN 2356–976x**
http://bjas.bu.edu.eg

Remote Sensing-Based Lithological Mapping of the Qena-Safaga Shear Zone Juxtaposing Northern and Central Tectonic Provinces of The Egyptian Nubian Shield

Asmaa.E.El-Araby[1*], Wael.D.Hagag[1], Samir.Z.Kamh[2] and Zakaria.E.Hamimi[1]
1 Geology Department, Faculty of Science, Benha University, Benha 13518, Egypt
2 Geology Department, Faculty of Science, Tanta University, Tanta 31527, Egypt
E-Mail: asmaageol@gmail.com

Abstract

Integration of remote sensing data (Landsat- 8, ASTER and Sentinel 2A) with field and petrographic studies is utilized to update the lithological/geological mapping of the central Qena-Safaga Shear Zone that juxtaposes the Northern Extensional Province against the Central Transpressional Province of the Egyptian Nubian Shield. The Neoproterozoic basement succession in the study area is classified into ophiolitic mélange, syn- tectonic granitoids, late- tectonic granitoids, Dokhan Volcanics and post- tectonic granitoids. These rock suits are dissected by NE-SW oriented dikes and NE-SW and NW-SE trending strike-slip faults. A number of remote sensing techniques (e.g., False Color Composites; FCC, Band Ratios; BR, Principal Component Analysis; PCA and Image Classification) were applied in the verification of the exposed litho-units. The FCC (RGB 7 5 3 for Landsat- 8 and 10 11 6 for Sentinel 2A), PCA (RGB 1 2 3, 3 2 1 and 6 4 3 for Landsat- 8; RGB 6 5 7 for Sentinel 2 A; and RGB 1 2 4 for ASTER), BR (RGB 4/3, 6/7, 6/5 for Landsat-8; and RGB 1/3, (5/3/+ ½), 5/7 for ASTER) and Supervised Classification including parallepiped method and Maximum Likelihood for Sentinel 2A are effective remote sensing techniques in rock discrimination. Besides, some alteration zones were recognized including phyllic (muscovite, b7/b6 for ASTER), ferrous silicates (chlorite, b5/b6 for Landsat-8), carbonate (calcite, b6/b7 for Landsat-8), kaolinite (b7/b5 for ASTER) and hydroxyl group (alunite, b4/b5 for ASTER). Such alterations exhibit bright pixels depending on the DN band threshold (DN band threshold= mean + 2* standard deviation).

Keywords: Qena-Safaga Shear Zone, Landsat-8, ASTER, Sentinel 2A, Mineral indices, Egyptian Nubian Shield

1. Introduction

The tripartite classification of the Eastern Desert [1-3] subdivided the Egyptian Nubian Shield in the Egyptian Eastern Desert into three tectonic terranes based on their lithological and structural variations, where the boundaries between these terranes are marked by megashears. Accordingly, the Eastern Desert was classified into North Eastern Desert (NED), Central Eastern Desert (CED) and South Eastern Desert (SED). The Qena-Safaga Shear Zone is one of the previously mentioned major shear zones . (Fig.1). It occupies the boundary between the NED and CED terranes. The present study is concerned with the geology of central part of such mega-shear zone (between latitudes 26° 20´ to 26° 40´N and longitudes 33 ° 10´ to 33 ° 35´E) through the processing of high resolution satellite images of Landsat-8, ASTER and Sentinel- 2A to distinguish between the different litho-units and major structural elements. Different algorithms have been applied on these images including False Color Composite, Principal Component Analysis and Band Ratioing, as well as image classification and mineral indices. Field and petrographical validation are used to assist and improve the results obtained from the processing of remote sensing data. Consequently, representative rock samples were carefully collected from the exposed litho-units, and petrographically investigated. Also, the lithological contacts between various litho-units have also been examined and mapped. The concerned area was the subject matter of several studies before, particularly in terms of geochemistry, petrology and mineralogy, as well as prospecting and exploration of gold and radioactive elements [4-6]. As a consequence, mapping of a large area as such introduced in the present study hasn't been considered before. The main aim of the present study is to update the geological map of the study area which is regarded as a transition zone between wrench-related tectonics in the CED to extensional tectonic regime in the NED [3].

2. Methods and data used

The present study is based essentially on the different remote sensing techniques which were used for discrimination between the different rock units in the study area (Fig.2). The remote sensing data used include Operational Land Imager (OLI) and Thermal Infrared Sensor (TIRS) of Landsat-8, Advanced Spaceborne Thermal Emission and Reflection Radiometer (ASTER) and Sentinel 2A. Firstly, these data are preprocessed and processed using different algorithms including False Color Composite (FCC), Principal Component Analysis (PCA) and Band

Ratios (BR), besides the Mineral Indices (MI). Image classification using Parallelepiped and Maximum likelihood algorithms was also used in this study. Processing of the data was carried out using some software, such as: ENVI 5.3, Erdas Imagine 9.2, SNAP Desktop 8 and ArcGIS (10.1).

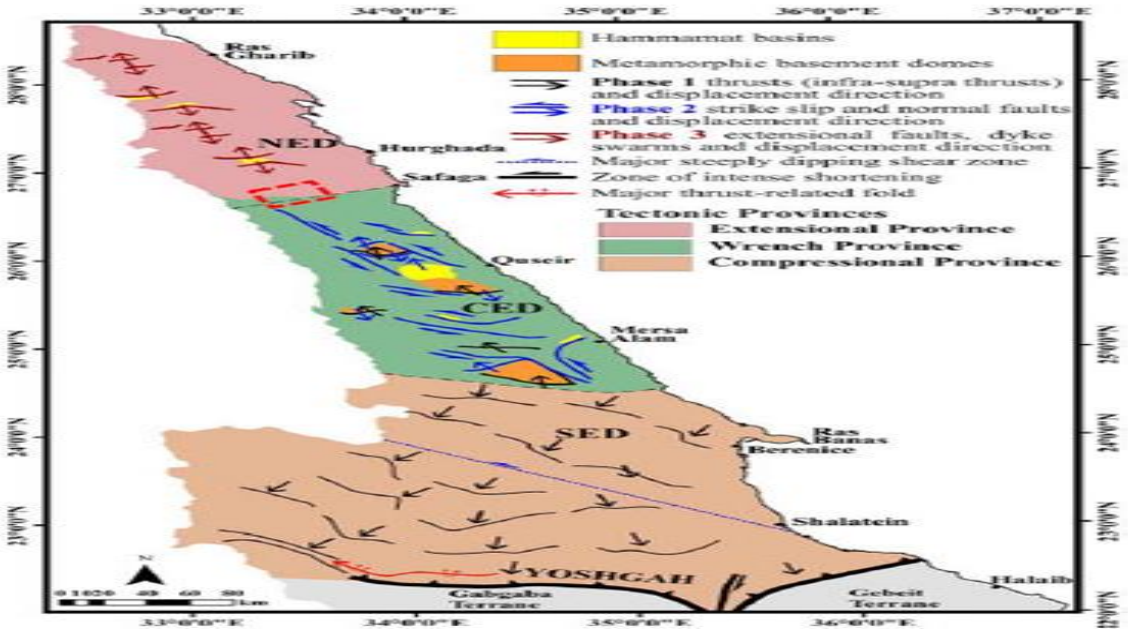

Fig(1) The three structural provinces of the Eastern Desert and the predominant structures within each domain (after [3]. NED: North Eastern Desert; CED: Central Eastern Desert; SED: South Eastern Desert. Red rectangle represents the study area.

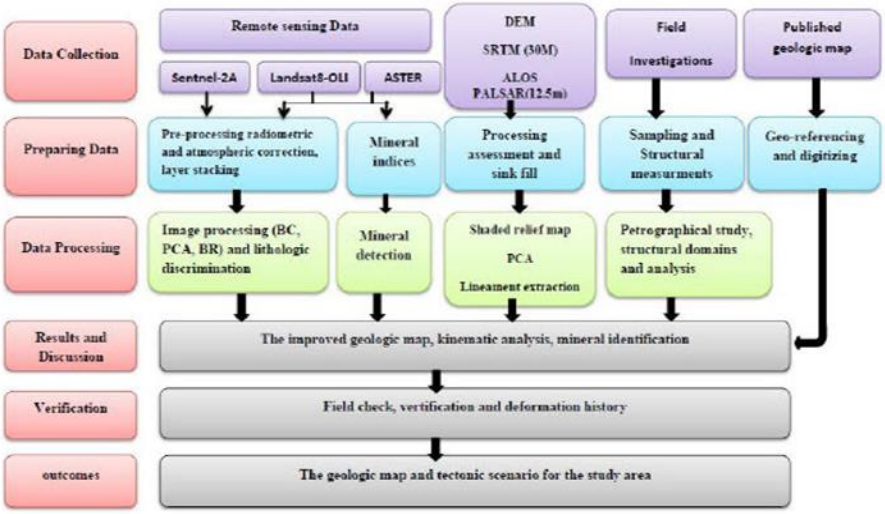

Fig (2) Flow chart of the different methods used in the present study.

2.1. Image pre-processing

Image preprocessing defines as image correction and rectification used for geometric and radiometric distortions of data of sensor and platform. In the present study, geometric and atmospheric correction of the raw data have been performed and followed by subsetting of the image to obtain the concerned area (the Central Qena-Safaga Shear Zone). Landsat-8 images are rectified geometrically to Universe Transverse Mercator (UTM) projection zone 36N and WGS 1984, while the Sentinel 2A and ASTER images are not corrected. Atmospheric correction is related to the radiometric correction as it helps to correct for a solar elevation and Earth – Sun distance difference. In

this study, atmospheric correction is performed by using several software including ENVI 5.3 and SNAP Desktop 8 software. Various algorithms have been used for the atmospheric correction including the Internal Average Relative (IAR) for Landsat-8 and Fast Line- Of – Sight Atmospheric Analysis of Hypercubes (FLAASH) algorithm for ASTER images while Sen3cor has been used for the correction of Sentinel-2A images.

2.2. Image processing and enhancement

Image processing is defined as processes applied on the images after the pre-processing. The main purpose of the image processing is to enhance the image and increase the visual interpretation of features on the image, and hence increasing the amount of information extracted. In the present study, different algorithms are used including Band Combination (BC), Principal Component Analysis (PCA), Band Ratioing (BR) and Mineral Index (MI). These techniques are very useful in lithological discrimination between the different rock units and also for identification of the alteration zones that can be used economically.

2.2.1. Principal Component Analysis (PCA)

Principal Component Analysis (PCA) is a statistical method used an orthogonal conversion to transform a data of correlated variables into a set of values of linearly uncorrelated variables. In this study, the FCC of PCA 1 2 3 of Landsat-8 has been used for discrimination between the younger granites that appear in green color including Gabal Rie El- Garra, Gabal El-Missikat, Gabal EL-Eridiya and Gabal Kab Amiri and older granites in greenish blue color in Gabal Semna (Fig 3a). The PCA 6 5 7 of Sentinel 2A differentiates the iron oxide alteration zones surrounding the Gabal Kab Amiri with pink color (Fig3b), while the differentiation between syn- and late- tectonic granitoids appears obviously through PCA 1 2 4 of ASTER (Fig.3c).

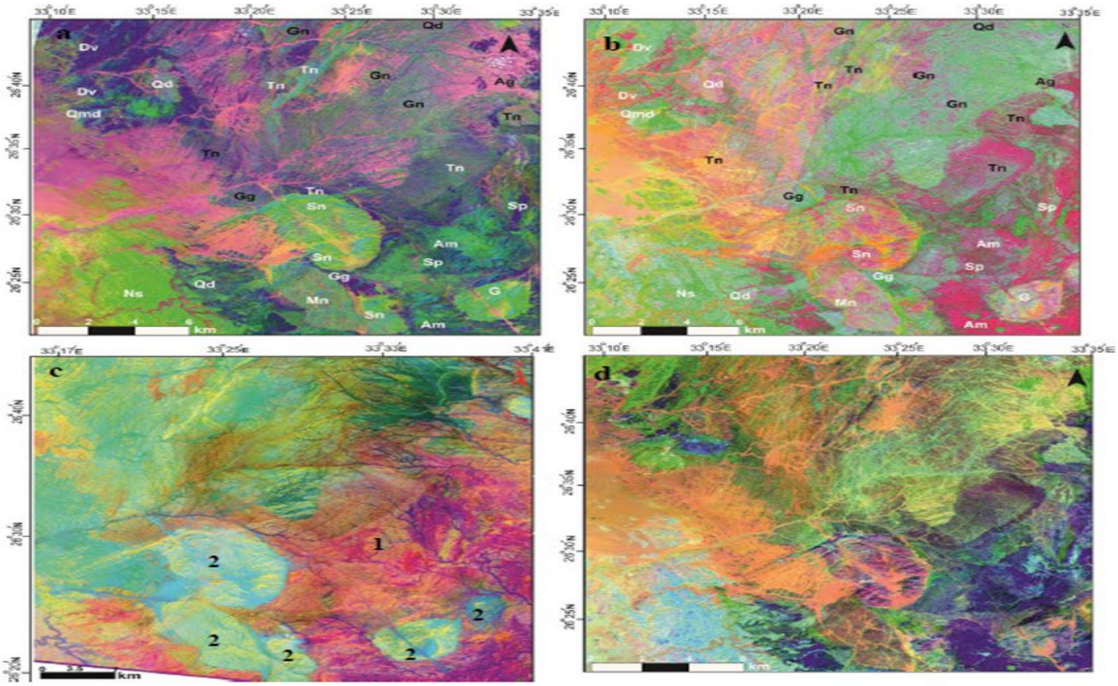

Fig (3) (a) PCA 123 RGB Landsat-8 image showing the different rock units in the study area. (b) PCA 657 RGB of Sentinel-2A image distinguishes the iron oxide minerals with pink color. (c) PCA 124 RGB image of ASTER where Syn-tectonic granites (1)(orange) are discriminated from late tectonic granites(2) (bluish yellow). (d) Band ratio combination RGB(4/3, 6/7, 6/5) of landsat-8 discriminate the late- tectonic granitoids in different locations (Rie El-Garra, El-Missikat , El- Maghrabiya and EL- Eridiya, Kab Amiri) in different color.

2.2.2. Band ratioing (BR)

Band ratioing (BR) is the process of dividing the DN value of one band by the DN value of the other band, where the pixel value in one band is divided by the pixel value in the other band [7-8]. We applied a number of band ratios to distinguish between the various lithologies in the study area, including RGB 4/3, 6/7, 6/5 for Landsat-8 .Fig 3d) which showed that

the late- tectonic granitoids in Gabal Ri El- Garra, Gabal El- Missikat, Gabal El- Maghrabiya differ in color from that in Gabal EL- Eridiya, Gabal Kab .Amiri suggesting diversity in the mineral composition or formed in different phases of deformation. The band ratio RGB (1/3, (5/3/+ ½), 5/7) of ASTER is used to distinguish the late- tectonic granitoids (appear in blue color, .Fig 4a) from the syn- tectonic granitoids.

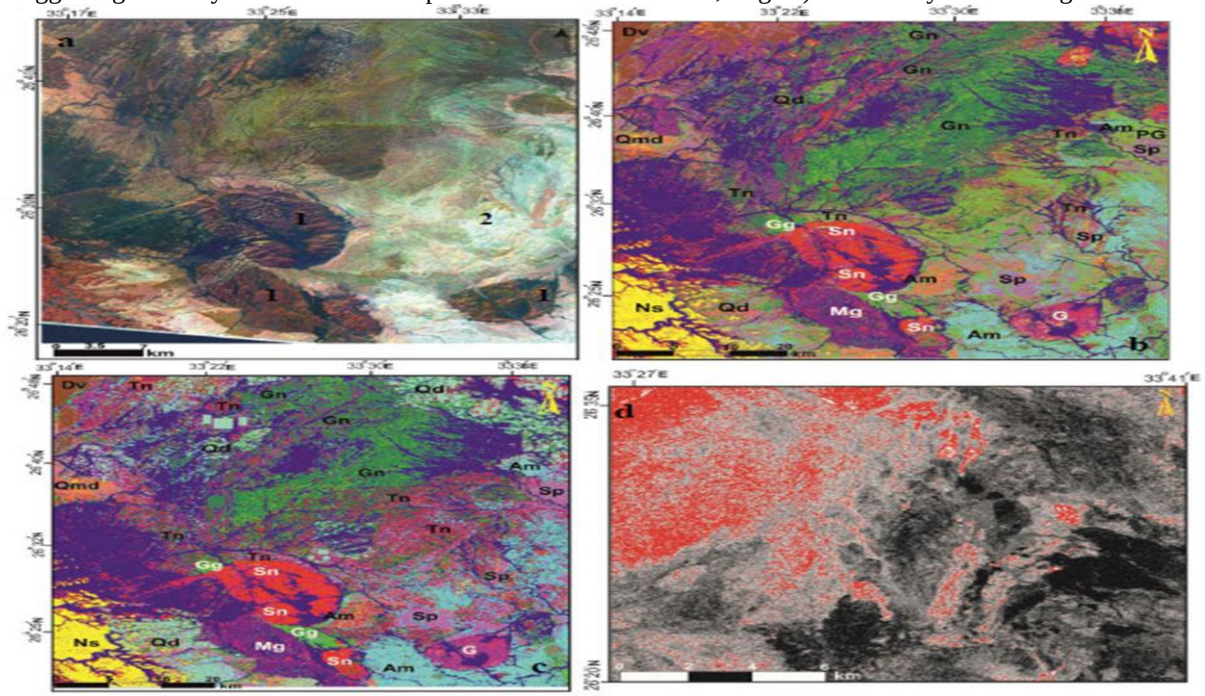

Fig (4) (a) Band ratio combination RGB (1/3, (5/3/+ ½), 5/7) RGB for ASTER separate the syn- tectonic granitoids (1) from late tectonic granitoids (2). (b) Classified image of Sentinel-2 based on parallepiped classification (c) Maximum Likelihood classification of Sentinel data. (d) ASTER band ratio b7/b6 threshold shows the distribution of muscovite minerals in Semna area.

2.2.3. Image Classification

The main objective of this classification is to put the common pixels with the similar spectral signature in particular themes or classes (e.g. water, forest, rock, etc.). The resulting map consists essentially of a mosaic of pixels, whereas each pixel belongs to a particular theme and represents a thematic map of the original image. We applied the supervised classification by using different algorithms such as parallelepiped and maximum likelihood.

Parallelepiped classification is an easiest method of supervised classification using a simple rule in the classification of the multispectral data. The idea of the parallelepiped classification depends on determination of the threshold of standard deviation from the mean of each selected class. The pixels that lie above the low threshold and below the high threshold for all n-bands are classified. If the pixel value falls in multispectral classes, ENVI assigns the pixel to the first class matched. Pixels that are not located within any of the parallelepiped described as unclassified.

Maximum likelihood classification is an algorithm supposedly that the statistics for each class in each band are distributed normally and calculates the probability that a given pixel belongs to a specific class. By selecting the threshold value, the pixels are classified. Each pixel is charged to class that has the highest probability (that is the meaning of the maximum likelihood). The pixels that having the threshold value smallest than the probability threshold becomes unclassified.

From the comparison between the results of parallelepiped and maximum likelihood methods, we recognized that the maximum likelihood results are better than the results extracted from the parallelepiped as all the rock units in the study area separated exactly in the case of the maximum likelihood .(Fig4 b,c) and also achieved through the calculation of the confusion matrix; with the overall accuracy is 100% and the kappa coefficient is 1 in the case of the maximum likelihood classification while the overall accuracy is 78% and the kappa coefficient is about 78% in the case of parallelepiped method.

2.2.4. Mapping mineralized zones in the study area (Mineral Index)

A wide variety of minerals have been identified in the concerned area, including quartz, chlorite, kaolinite, sericite, pyrite, chalcopyrite, alunite and

calcite. Alteration zones associated with gold mines have been identified by the iron oxide minerals that are associated with uranium through the mineral indices for Landsat-8, ASTER and Sentinel 2A. The ASTER index for minerals is applied to characterize these alteration zones include B7/B6 that is useful for discrimination of the muscovite minerals [9] in the Semna area Fig.4d). Kaolinite is discriminated by B7/ B5 . 5a) Alunite minerals .5b) are differentiated by B4/B5 .Despite the success of ASTER band ratioing in distinguish some minerals such as muscovite, kaolinite and alunite, but it fails to distinguish some others such as chlorite and calcite where Landsat-8 proved its effectiveness in identifying chlorite by applying B5/ B6 .Fig5c) [10] and calcite by B6/B7 Fig.5d) [11].

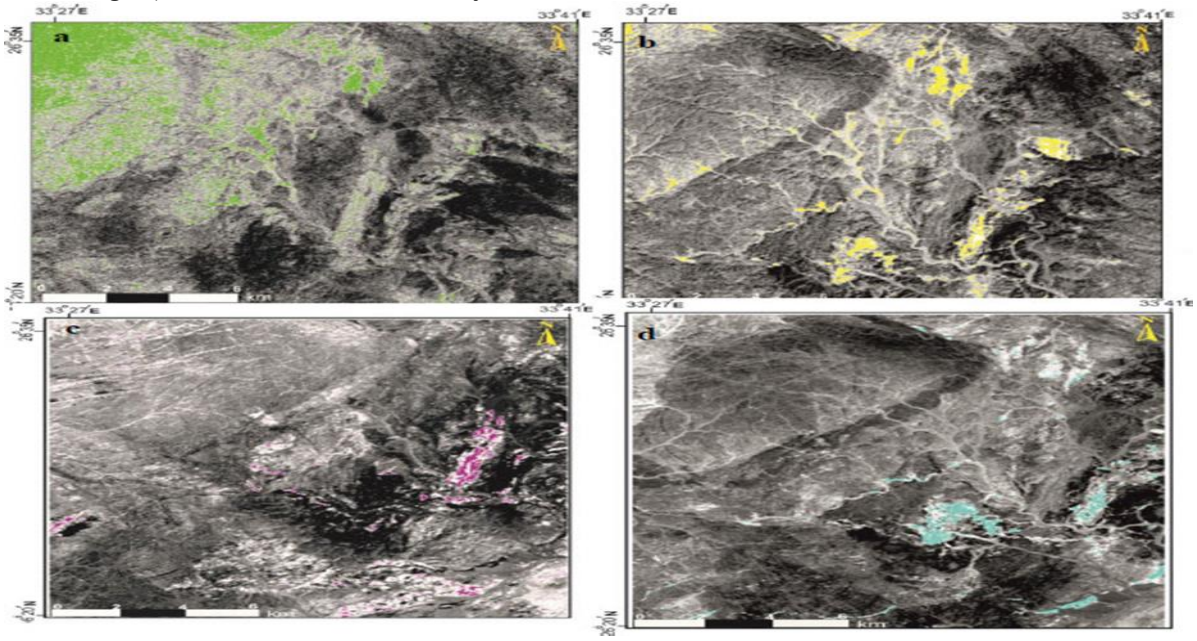

Fig (5) (a)**.** ASTER band ratio b7/b5 threshold shows distribution of kaolinite minerals in Semna area. (b) ASTER band ratio b4/b5 threshold shows the distribution of Alunite minerals in Semna area. (c) Landsat-8 band ratiob5/b6 threshold appears the chlorite minerals in Semna area. (d) Landsat-8 band ratiob6/b7 threshold shows the distribution of calcite minerals in Semna area.

3. Field and petrographic validation

The study area is characterized by rough topography with moderate to high relief ground surface including different basement units of Neoproterozoic age, covered by Phanerozoic Nubian Sandstone. Depending on the remote sensing-based lithological discrimination, field studies and petrographic examination, the different litho-units in the study area are mapped Fig.6). These rock units are arranged geochronologically from oldest to youngest as follow: (1) Metaultramafics, (2) Amphibolites, (3) Syn- tectonic granitoids (gneissose granite, tonalite, quartz diorite and granodiorite), (4) Late- tectonic granitoids (quartz monzodiorite, monzogranite, syenogranite and granite), (5) Dokhan Volcanics, and (6) post- tectonic granites. These units are intruded by basic, intermediate and acidic dykes, and unconformably overlain by the Nubian Sandstones to the west.

3.1. Metaultramafics (Serpentinites)

The metaultramafics are mainly serpentinites which are fine-grained with greenish black color and characterized by mesh texture. They are encountered at the southeastern part of the study area where they exposed next to the Kab Amiri pluton from the north, south and east. They are foliated, sheared and intersliced with talc carbonate sheets (Fig.7a). Petrographically, metaultramafics are composed mainly of antigorite, tremolite, carbonates and talc, while opaque minerals are accessories (Fig.7b).

3.2. Amphibolites

Amphibolites are distributed in the southeastern and central eastern parts of the study area. They crop out at the eastern part of El-Eridiya pluton, where they are foliated and fine- grained with dark green color, and contain offshoots of the syenogranites of El-Eridiya pluton (Fig.7c). The amphibolites are composed predominantly of amphiboles and relics of pyroxene minerals with plagioclase embedded between the other constituents (Fig.7d).

3.3. Syn-tectonic granitoids

According to field observations and petrographic characteristics, the syn-tectonic granitoids are classified into gneissose granite, tonalite, quartz diorite and granodiorite. These rocks are exposed in the form of variably-sized plutons distributed all over the study area.

Gneissose granites

They are located to the northwest of Rie El-Garra and south of El-Gidami granitic plutons. Northwest of Rie El-Garra, the granites are generally coarse-grained with distinctive grey color and characterized by gneissosity and mylonitization with the presence of quartz porphyroclasts (Fig.7e). The gneissose granites are biotite-hornblende gneissose granites (Fig.7f).

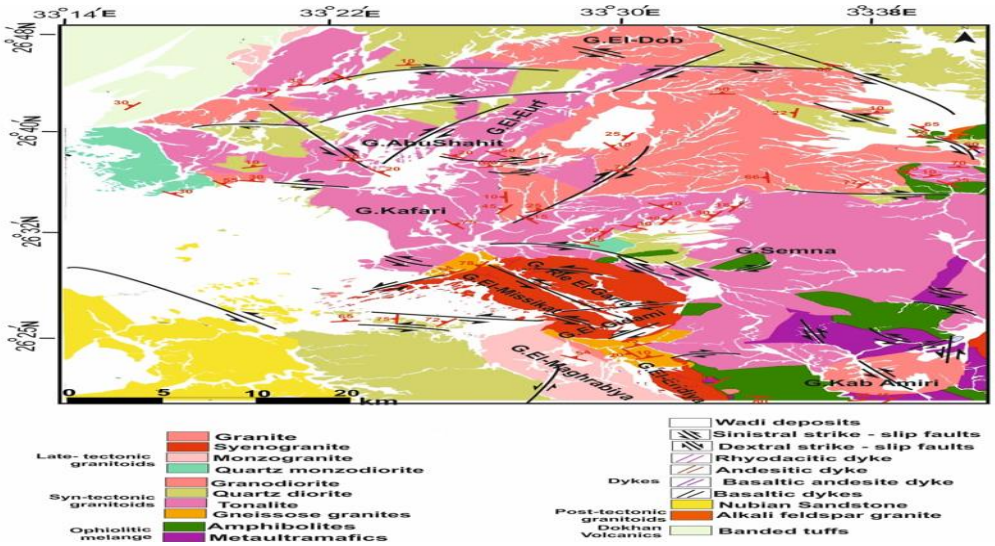

Fig (6) Geologic map of the study area (constructed based on image processing of Landsat-8, ASTER, Sentinel2 A data, besides the field/structural work and ground truth).

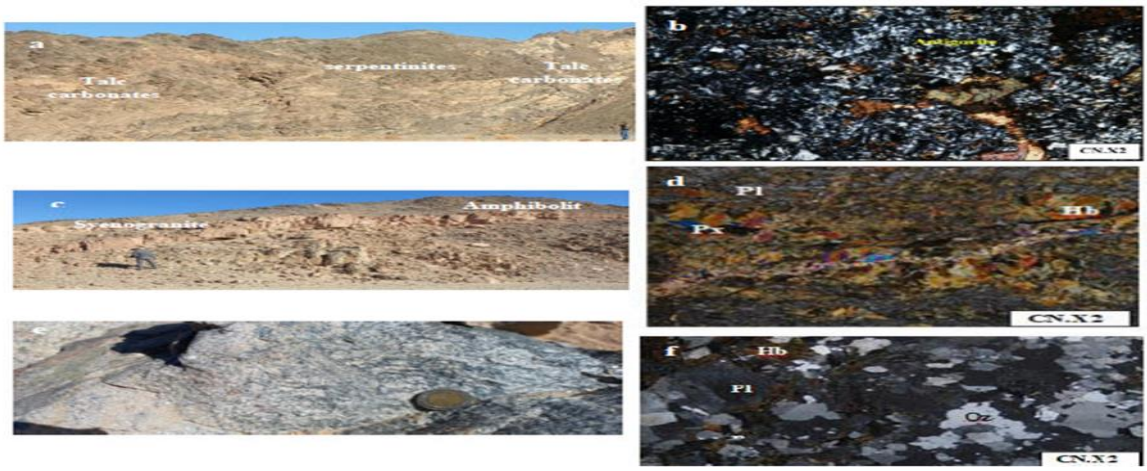

Fig (7) (a) Alteration of serpentinite rocks into talc carbonates due to retrogressive metamorphism, south to Kab Amiri pluton (b) Photomicrograph showing antigorite fibrous in the serpentinites, located south to Kab Amiri pluton (c) Offshoots of EL- Eridiya syenogranites intruding the Amphibolites, (d) Photomicrograph of amphibolitic rocks east to El-Eridiya pluton composed essentially of hornblende (with pyroxene relics) and plagioclase (e) General view of gneissose granite in the northern part of Rie El-Garra pluton showing gneissosity and quartz porphyroclasts, (f) Photomicrograph showing biotite-hornblende gneiss, composed mainly of quartz, biotite, hornblende, plagioclase minerals located at the north western part of Gabal Rie El-Garra

Tonalite

The tonalitic rocks occupy vast domain in the study area constituting different plutons in Semna, Kafari, El-Eurf and Abu Shahit. They are undeformed and coarse-grained with grayish-white color, as well as exfoliated and containing amphibolite enclaves Fig. 8a). Theyconsist mainly of quartz, plagioclase, perthite, biotite and hornblende .Fig. 8b).

Quartz diorite

Quartz diorites form a small belt east of Rie El-Garra pluton. These rocks are exfoliated and coarse-grained with grayish-white color. They were affected by shearing and traversed by basaltic dykes . Fig.8c). Quartz diorites are composed of plagioclase, hornblende, perthite, orthoclase and biotite, with minor quartz Fig. 8d).

Granodiorite

Various plutons are made up of granodiorites. These plutons are typified by El-Dob pluton that is encountered in the north-central part of the study area. They form an elongated mass located to the north of Gabal Semna, in the northeastern corner of the study area .They are coarse-grained with grey color. They are sheared, exfoliated and characterized by gneissose texture . Fig.8e). Granodioritic rocks are characterized by perthitic texture . Fig.8f) and composed essentially of quartz, plagioclase, microcline- perthite and orthoclase, with biotite and hornblende.

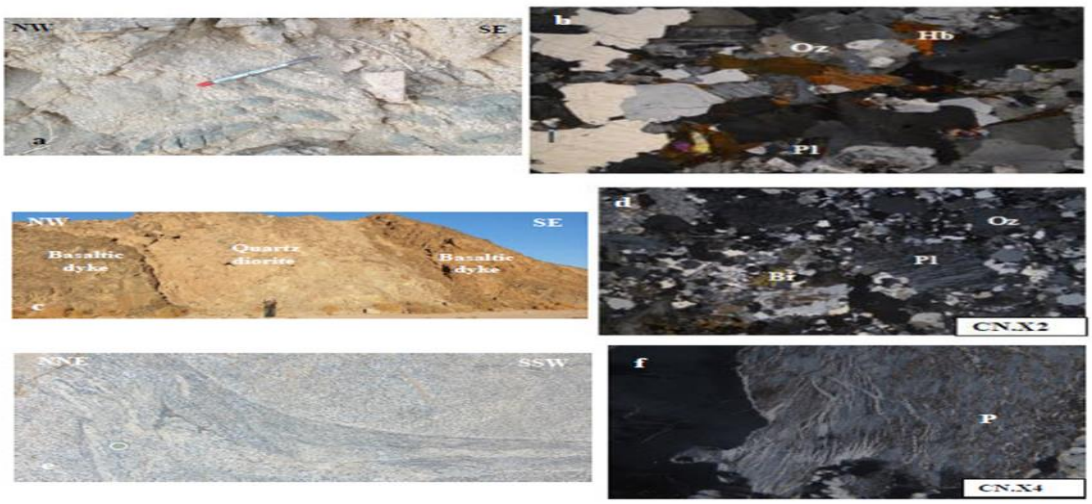

Fig (8) (a) Amphibolite enclaves within the tonalite rocks of Gabal Semna (b) Photomicrograph of Semna tonalitecomposed of subhedral crystals of plagioclase, quartz, biotite and hornblende.(c) Sheared quartz diorite east of Rie El-Garra pluton dissected by basaltic dykes (d) Photomicrograph of quartz diorite located to the northeast of Rie El-Garra pluton showing subhedral crystals of quartz (Qz), plagioclase (Pl), perthite (P) and biotite (Bi). (e) Remarkable gneissosity in the granodiorites to the north of Gabal Semna (f) Photomicrograph showing well developed perthitic texture in El-Dob granodiorites .

3.4. Late-tectonic granitoids

In the study area, the late-tectonic granitoids are represented by quartz monzodiorite, monzogranite, syenogranite and granite.

Quartz monzodiorite

The quartz monzodiorite forms two granitic plutons located to the northeast of Rie El-Garra and northwest of Gabal Kafari. It is massive and coarse-grained with greyish white color Fig.9a). Microscopically, it is composed essentially of plagioclase, hornblende, orthoclase and biotite, with minor quartz crystals. The alteration products include sericite, kaolinite, muscovite, epidote, carbonate and chlorite. Plagioclase occurs as colorless tabular crystals altered to sericite and kaolinite, displaying zoning and showing micrographic texture Fig.9b).

Monzogranite

The El-Maghrabiya pluton is composed essentially of monzogranite. The monzogranite is massive with reddish pink to pink color and medium- to coarse-grained texture. It is mylonitized and characterized by compositional banding Fig .9c). Petrographically, the it consists mainly of quartz, plagioclase, microcline, biotite and hornblende Fig.9d).

Syenogranite

Synogranite is common in the study area. It has a general moderate to high relief with steep slopes and is represented by four main plutons, namely Gabal El-Missikat, Gabal Rie El-Garra, Gabal El-Gedami and Gabal El-Eridiya. In El-Missikat pluton, the syenogranite is sheared, mylonitized and pegmatitized

with reddish pink to pink color and medium to coarse-grained texture. It contains xenoliths of older granitoids and metavolcanics varying in shape and size with different degrees of assimilation and digestion Fig.9e). It is composed essentially of quartz, plagioclase, perthite and biotite. The alteration products include chlorite, muscovite, sericite and kaolinite. Quartz crystals occur as irregular coarse and fine crystals between the other constituents and characterized by undulose extinction and hourglass texture Fig .9f).

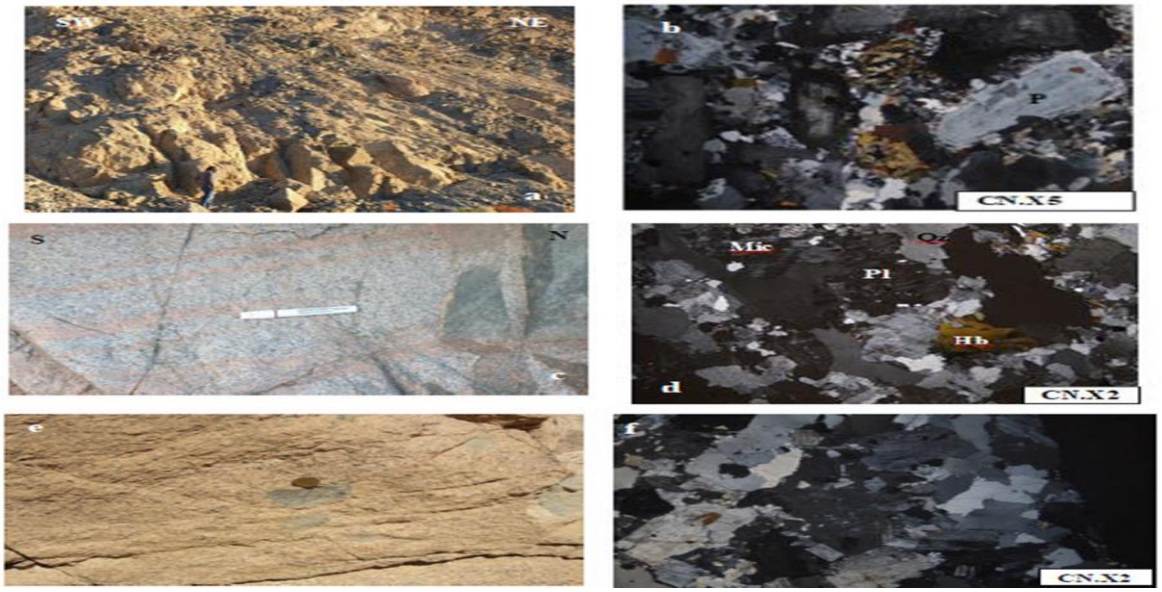

Fig (9) (a) An outcrop of quartz monzodiorite located at the north east of G.Rie El-Garra. (b) Photomicrograph showing zoned plagioclase crystals and micrographic texture in the quartz monzodiorite located to the west of G. Kafari., (c) Banded monzogranite in the El-Maghrabiya pluton. (d) Photomicrograph showing themineral composition of El-Maghrabiya monzogranite including plagioclase, microcline, perthite, quartz with biotite and hornblende. € Xenoliths of older granite and metavolcanic inside the syenogranites of El-Missikat pluton (f) Photomicrograph showing hourglass texture in the quartz crystals of Rie El-Garra syenogranite.

Granite

The Kab Amiri pluton consists almost entirely of coarse grained exfoliated granite Fig.10a). Under the microscope, it is identified as biotite granite being composed mainly of quartz, plagioclase, microcline, perthite and biotite Fig.10b).

3.5. **Dokhan Volcanics**

The Dokhan Volcanics are represented by banded tuffs Fig.10c) which is located in the northwestern part of the study area. Microscopically, the banded tuffs are composed essentially of crystal- and rock- fragments. The crystal fragments comprise plagioclase and quartz that are embedded in a fine-grained groundmass of the same constituents. These rocks are distinguished by banding Fig.10d).

3.6. **Post- tectonic granites**

alkali feldspar granites

The alkali feldspar granites are cropping out at the northeastern part of Gabal Semna. They are coarse-grained with pink color, sheared and intruded in the amphibolite rocks Fig.10e). Microscopically, quartz and perthite are the main constituents of the alkali-feldspar granite. Quartz forms shapeless crystals displaying the wavy texture. Perthitic texture do exist Fig.10f).

3.7. Felsic to mafic dykes

The above mentioned litho-units are traversed by various types of dykes, ranging in composition from mafic to acidic (i.e. basalt, basaltic andesite, andesite, rhyodacite and rhyolite). The main trends of mafic dykes are NE-SW, WNW-SSE and E-W, parallel to the main trends of faults, and most of them are nearly vertical. The basaltic to basaltic andesite dykes dissect the tonalite rocks located at the eastern part of Gabal Kafari Fig.11a). Under the microscope, the andesitic dykes are composed of plagioclase and hornblende. The secondary minerals include sericite, kaolinite and chlorite. Opaques are the main accessories Fig.11b).

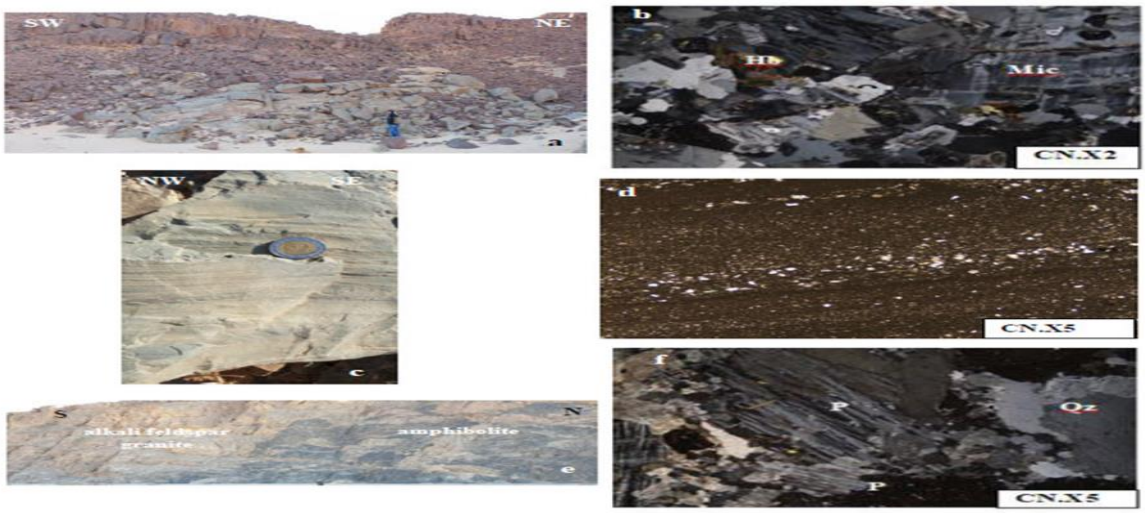

Fig (10) (a) Exfoliated granite in Kab Amiri pluton, (b) Photomicrograph showing the main composition of Kab Amiri granite, (c) Banded tuffs located north western part of the study area (d) Photomicrograph showing banding in tuffs encountered to the west of Gabal Kafari (e) Sheared alkali -feldspar granite intruding amphibolites at the northeastern part of Gabal Semna. (f) photomicrographic showing that alkali- feldspar granite composed essentially of subhedral quartz and perthite crystals.

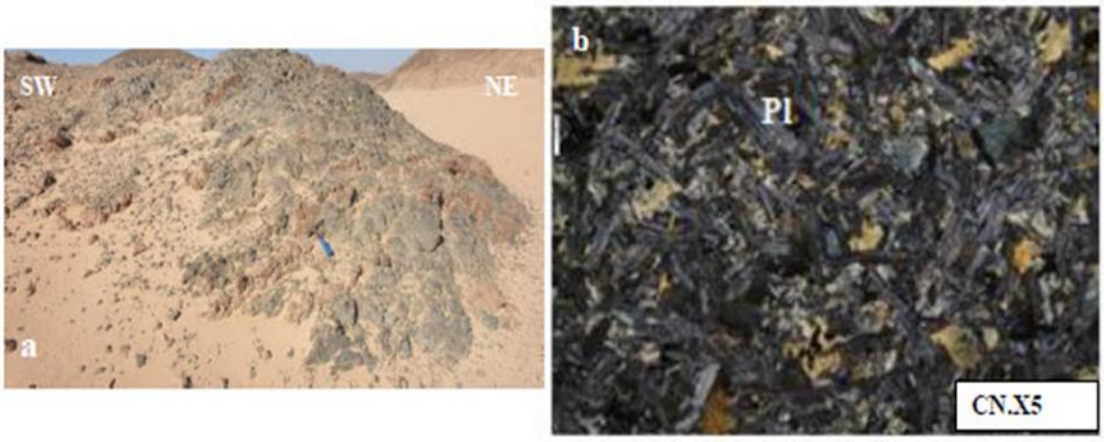

Fig (**11) (a)** Swarms of basaltic dykes cutting granodiorite located east to Gabal Kafari. (b) Photomicrograph showing the main composition of basaltic dykes of north eastern part of Gabal Semna.

4. Summary and conclusions

The present study introduces an integrated approach utilizing remote sensing, field work and petrographic study in order to update the geological map of one of the key areas in the Egyptian Eastern Desert, namely the central Qena-Safaga Shear Zone. This zone juxtaposes the CED and the NED. The applied remote sensing methods are particularly contributed to the discrimination of the different Neoproterozoic basement rock units and regionally to the geology of the studied area through consistent field and petrographic study. In conclusion, the earlier rock units and associated geological structures are highly masked by the later magmatic activity which was mainly represented by the intrusion of a series of syn-tectonic, late- tectonic to post- tectonic granitoids of various compositions. Therefore, the present study suggests that the NED was strongly affected by extensional-transtensional tectonic regime following the compressive to transpressive tectonic movements that were predominated during and just after the convergence between East and West Gondwana.

References

[1] S. El-Gaby, Architecture of the Egyptian basement com-plex. IBTA Association, Publ. (5), pp.1–8,1983.

[2] R.O. Greiling, M.M. Abdeen, A. A. Dardir, H. El Akhal, M.F. El Ramly, G.M. KamalEl Din, A. F. Osman, A.A. Rashwan , A. H. N. Rice and M. F. Sadek, A structural synthesis of the Proterozoic Arabian-Nubian Shield in Egypt. Int. J. Earth Sci., Vol.83,pp.484-501, 1994.

[3] Z. Hamimi, W. Hagag, H. Fritz, H. Baggazi, S. Kamh, The Tectonic Map and Structural Provinces of the Late Neoproterozoic Egyptian Nubian Shield: Implications for Crustal Growth of the Arabian–Nubian Shield (East African Orogen). Front. Earth Sci. 10:921521. https://doi.org/10.3389/feart.2022.921521, 2022.

[4] F. Khaleal, Granites of Gabal El- Dob area and associated pegmatites, Central Eastern Desert. NSSJ, Vol.3, pp.15-25,2014.

[5] O.M. Draz, S.M. El Alfi and E.M. Esmail, Mineralogical and Radiometrical studies of Gabal El-Dob area, Central Eastern Desert, Egypt. Curr. Sci. Int,Vol.6, pp. 103 -120, 2017.

[6] A.M. Eldosouky, R.A. El-Qassas, A.B. Pour, H. Mohamed and M. Sekandari, Integration of ASTER satellite imagery and 3D inversion of aeromagnetic data for deep mineral exploration, pp.1-22, 2021.

[7] T.M. Lillesand, R.W. Kiefer, Remote sensing and image interpretation. John Wiley & Sons, Inc.,736 p, 1979.

[8] Khaleal, Granites of Gabal El- Dob area and associated pegmatites, Central Eastern Desert. NSSJ, Vol.3, pp.15-25,2014.

[9] R.D. Hewson, T.J. Cudahy, and J.F. Huntington, Geologic and alteration mapping at Mt Fitton, South Australia, using ASTER satellite-borne data.' IEEE 2001 International Geoscience and remote sensing Symposium (IGARSS), 9-13 July, 2001.

[10] H. Ghrefat, A. Kahal, K. Abdelrahman, H. Alfaifi and S. Qaysi, Utilization of multispectral landsat-8 remote sensing data for lithological mapping of southwestern Saudi Arabia. J. King Saud Univ. Sci..Vol.33,2021.

[11] S. E.skandari, H.R. Pourghasemi and J. Tiefenbacher, Relations of land cover, topography, and climate to fire occurrence in natural regions of Iran: Applying new data mining techniques for modeling and mapping fire danger**.** For. Ecol. Manag,Vol. 473,2020.